Macromolecules

Article

pubs.acs.org/Macromolecules

# Pressure Quench of Flow-Induced Crystallization Precursors

Zhe Ma,[†,‡] Luigi Balzano,[†,‡,§] and Gerrit W. M. Peters*[,†,‡]

[†]Department of Mechanical Engineering, Eindhoven University of Technology, P.O. Box 513, 5600MB, Eindhoven, The Netherlands

[‡]Dutch Polymer Institute (DPI), P.O. Box 902, 5600AX, Eindhoven, The Netherlands

Supporting Information

**ABSTRACT:** We developed a novel protocol to study the mutual influence of shear flow and pressure on crystallization of polymers. Here, we have applied this protocol, named "pressure quench", to polyethylene with a bimodal molecular weight distribution. With pressure quench, the undercooling, required to initiate crystallization of flow-induced precursors generated at high temperature, is obtained by increasing pressure, i.e., leaving the specimen isothermal. We find that pressure enhances the effect of shear. In particular, results show that the pressure quench effectively "lightens up" shear-induced precursors which otherwise are not observable, even with high-resolution synchrotron X-ray scattering. A pressure quench in combination with SAXS and WAXD gives insight into the early stages of crystallization. In this paper we focus on the use of WAXD since it provides all the information required to demonstrate our main issues. We conclude that precursors with different stability can be formed during shear and, with annealing, the least stable ones relax back to the melt. Finally, it is demonstrated that when pressure is released after crystallization, an "inverse quench" takes place and crystalline structures partially melt, similar to an increase of the temperature.

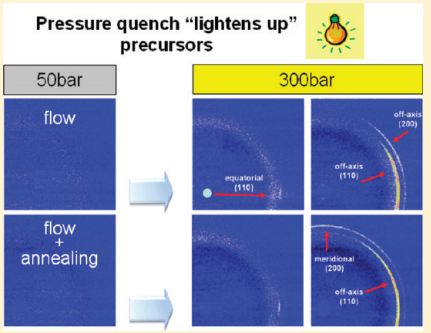


## 1. INTRODUCTION

Semicrystalline polymers represent the largest group of commercial polymeric materials. Their properties strongly depend on the crystalline structures that form during processing.[1−4] Apart from molecular features, the structures formed are controlled by processing variables such as flow, pressure, and temperature. These variables are often investigated individually, but there is also a remarkable mutual influence that is still unexplored. Laying ground for unraveling the relation between pressure and flow is the topic of this paper.

It is established that shear flow is able to generate precursors of crystallization in molten polymers.[5−8] Flow-induced precursors are metastable domains where stretched molecules assume a packing order in between the amorphous and the crystalline state. They can be considered as the cradle of flow-induced nuclei as, in suitable conditions, e.g. at low temperature, they nucleate and grow into crystalline structures. In this way, crystallization kinetics is accelerated, and the final morphology of the material is altered. Therefore, monitoring formation and evolution of crystallization precursors is crucial to rationalize the effect of flow on the final morphology of polymeric manufactures.

Precursors are often invisible to scattering techniques such as SAXS and WAXD because their structure is neither crystalline nor densely packed or their concentration is too low to produce significant effects. In these cases, they are studied indirectly by interpreting features (such as kinetics and morphology) of the subsequent crystallization process.[9−15] Interestingly, precursors can be generated and survive for long times also when temperature is around and sometimes above the melting point.[9,11−14] Especially in these cases, cooling to a lower temperature is a convenient way to trigger crystallization. For instance, Hsiao et al.[9] found that, for polyethylene (PE), after flow ($\dot{\gamma}$ = 12 s, $t_s$ = 12 s) at 134 °C, no structure could be observed with WAXD. Nevertheless, after bringing the system at 129 °C, oriented crystals started to grow. Practically, the cooling step should be fast and the final temperature not too low in order to keep the nucleation and growth separated on the time resolution of the experiment. This is commonly achieved by cooling with a liquid or gas medium. Small lab-scale devices, such as the commercially available Linkam shear cell, can reach cooling rates up to 30 °C/min.[14] Whereas, flow cells designed for strong flows and high pressures are typically restricted to lower values as they are constructed out of relatively large masses of metal. For example, the average cooling rate for the original design of the Multi-Pass Rheometer (MPR) is 1 °C/min.

When performing flow around the melting point followed by cooling to a lower temperature, the lifetime of precursors becomes an important parameter as for long cooling times (compared with the lifetime); a fraction of the precursors dissolves and thus mitigates the apparent effect of flow on crystallization. Balzano et al.[16] suggested that, shortly after flow unstable precursors dissolve on the time scale of the reptation of the longest molecules of the melt. Therefore, experimental protocols are required that allow for studying the details (number, size, morphology, and dynamics) of precursors in the

Received: December 19, 2011
Revised: April 13, 2012

  

very early stages while having control over their relaxation behavior. The goal is to separate the nucleation from the growth step. In this light, cooling directly to room temperature is often not a valid option since the fast overgrowth of crystalline structures would obscure nucleation. On the other hand, performing experiments at high temperature, close to the nominal melting temperature, seems a better solution as growth is very slow in these conditions. The drawback is that structures created at high temperatures are very sporadic and easily fall beyond the detection limits even of high-resolution methods such as synchrotron X-ray scattering.

An alternative way to perform controlled quenching is to utilize a pressure quench. In other words, apply pressure and, in this way, shift the melting temperature (according to the Clausius−Clapeyron relation) and thus effectively increase the undercooling without actually changing the sample temperature. This methodology can be directly implemented in certain slit-flow devices such as the one developed in Eindhoven[17] (mounted on the MPR) and offers some clear advantages: (i) The cooling step can be instantaneous. (ii) Temperature gradients and undershoots can be avoided (especially important for thick samples). (iii) The cooling step is easily reversed by depressurizing so complex undercooling histories can be applied simply by varying pressure.

Pressurization has been used as an alternative way to shift the phase boundary in studies on phase separation.[18,19] In particular, it was found that during phase separation of polymer blends the general features of nucleation are independent of whether the undercooling is obtained by decreasing temperature or by increasing pressure.[19] Therefore, pressure quench provides an effective way to obtain undercooling. Moreover, it also reflects the practically important, mutual influence between flow and pressure in polymer processing techniques.

In this paper, we demonstrate the use of pressure quench to investigate the early stages of nucleation of flow-induced precursors. We focus on a model bimodal blend of PE containing 3 wt % high molecular weight tail to simplify the rheological classification[20] of the flow conditions and to enhance the flow-induced formation of crystallization precursors.[21−27] Only a relatively mild increase of pressure is used in this work, since a few degrees of undercooling is already effective to accelerate the flow-induced crystallization growth. Moreover, a too high pressure (on the order of kbar) may induce the hexagonal phase[28,29] of PE, which is beyond the scope of this work.

Theoretical aspects on the origin of flow-induced precursors are not discussed here. Details can be found in a previous paper of our group.[30] For example, the issue if flow creates precursors directly from the melt or if they are always present, i.e., dormant precursors, see refs 31 and 32, and only their size is changed by the flow which increase the number that can be activated by a quench, was dealt with in detail.

## 2. EXPERIMENTAL SECTION

**Materials.** A bimodal polyethylene blend containing 3 wt % of high molecular weight tail was used in this work. The ultrahigh molecular weight polyethylene (UHMWPE) has a weight-averaged molecular weight $M_w$ = 1480 kg/mol and polydispersity $M_w/M_n$ = 2.[33] The linear low molecular weight polyethylene (LMWPE) matrix, supplied by Basell Polyolefine GmbH (Frankfurt, Germany), has a $M_w$ = 45 kg/mol and polydispersity $M_w/M_n$ = 3. The critical overlap concentration of high molecular weight molecules can be calculated with[34,35]

$$c^* = \frac{3M_w}{4\pi\langle R_g^2\rangle^{3/2}\rho N_A} \quad (1)$$

where $\langle R_g^2\rangle$ is mean-square radius of gyration of chain related to the molecular weight by $\langle R_g^2\rangle^{1/2} = 0.46M_w^{1/2}$,[36] $\rho$ is the density and $N_A$ is Avogadro's number. The estimated critical concentration of UHMWPE is around 0.35 wt %, i.e., much smaller than the 3 wt % in bimodal blend, meaning that a significant number of entanglements exist between the UHMWPE molecules.

**Sample Preparation.** The bimodal system was prepared by solution blending to achieve mixing at a molecular scale. The UHMWPE was first dissolved in a xylene solution at 130 °C, and subsequently LMWPE was added to dissolve, where the concentration of total PE's is 2.5% with an antioxidant (IRGANOX1010) added at a concentration of 2000 ppm. This solution was stirred for 1 h under a nitrogen atmosphere. Next, the hot xylene solution was poured into a large excess of stirred cold methanol. The precipitated gel was filtered and washed with methanol several times and then dried in vacuum at 80 °C for 2 days. After further addition of 2000 ppm of antioxidant (IRGANOX1010), in order to avoid degradation during sample preparation, the bimodal blend was compression molded at 160 °C into strips to fit the test cell.

**Experimental Protocol.** The slit flow device developed in Eindhoven[17,37] is an evolution of the Multi-Pass Rheometer of Eland Engineering Co Ltd. (UK)[38] (see Figure 1). The flow cell is specifically designed for online scattering and therefore equipped (at the center) with diamond windows (opening angle of 45°). The specimen ($L$ = 200 mm, $W$ = 6 mm, and $H$ = 1.5 mm) is confined between two servo hydraulically driven rectangular pistons. An important advantage of this slit-flow device is the possibility to impose and release pressure. The maximum pressure is 800 bar and the maximum temperature 250 °C. The procedures for flow, pressurization, and depressurization are illustrated in Figure 1.

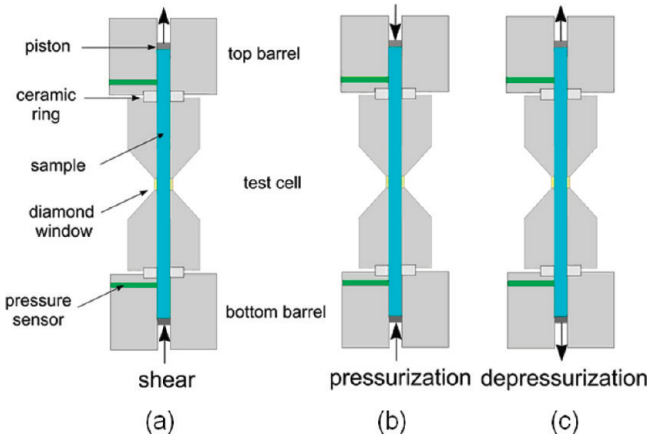


**Figure 1.** Schematic of the flow device and flow, pressurization, and depressurization procedures. Moving directions of the pistons are indicated by arrows. Heating rods and the heating/cooling channels are not shown.

Moving the two pistons in the same direction introduces a shear flow to the sample (Figure 1a), while moving the two pistons toward or away from each other will pressurize (Figure 1b) or depressurize (Figure 1c) the sample, respectively, without causing any flow at the observation point (center of the slit). The pressure difference during flow is recorded by means of two pressure transducers.

The experimental protocol used in this paper is shown in Figure 2. The polymer in the test cell is first heated up and annealed at 190 °C for 10 min to erase the memory of previous thermal and mechanical histories and then cooled to 134 °C at which shear, pressurization, and depressurization are performed. To avoid temperature fluctuations, the cell is stabilized by means of an oil bath, while the top and bottom


dx.doi.org/10.1021/ma2027325 | Macromolecules XXXX, XXX, XXX−XXX

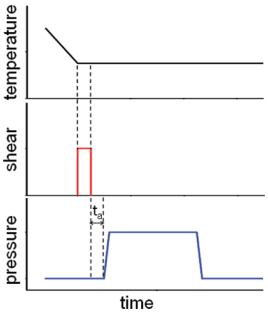


**Figure 2.** Experimental protocol. The annealing time $t_a$ is between cessation of flow and pressurization.

barrels are always kept at high temperature (190 °C) in order to have the pressure transducers functioning properly. Next, flow is imposed with a piston speed of 15 mm/s for 0.8 s. The shear rate and Weissenberg number ($Wi$) distributions over the slit thickness were estimated considering the rheology of the material and are shown in Figure 3 (see also the Supporting Information). The shear rate varies nonlinearly from 0 at the slit center to a maximum of 67 $s^{-1}$ at the wall. The Weissenberg number, $Wi = \dot{\gamma}\tau_{Rouse}$, is used to estimate the molecular stretch induced by flow. When $Wi > 1$, molecules become stretched, and this is a requirement for the creation of precursors.[39] The longest Rouse times of UHMWPE and LMWPE at 134 °C are 4.9 × $10^{-2}$ and 4.5 × $10^{-5}$ s (see section 3.3 for the calculation), respectively, so the Weissenberg number for molecular stretch at the wall is 3.3 for HMW tail but nearly zero for LMW matrix.

In order to obtain good filling of the slit and rule out wall slippage, a reference pressure of 50 bar was kept on the specimen. The average pressure during flow, $P_{Average} = {}^1/_2\Delta P_{sensor}$, where $\Delta P_{sensor}$ is the pressure difference between the two pressure sensors, is around 55 bar, so the influence of flow on the pressure level is negligible. A pressure of 300 bar was chosen as the elevated pressure level to increase the melt undercooling. Figure 2 also shows that pressurization can be applied right after flow ($t_a = 0$) or after annealing ($t_a = 22$ min) with the same flow. Both protocols were employed in this work. The former ($t_a = 0$) is used to see if any precursors were formed during flow, and the latter ($t_a = 22$ min) is to show how precursors develop with time.

**X-ray Characterization.** X-ray measurements were carried out at the Dutch-Belgian (DUBBLE) beamline BM26 of the European Synchrotron Radiation Facility (ESRF) in Grenoble, France, with a wavelength of 0.95 Å. A Frelon detector with a resolution of 2048 × 2048 pixels of 48.8 $\mu$m × 48.8 $\mu$m, and placed at a distance of 0.195 m, was used for wide-angle X-ray diffraction (WAXD). The measuring time of each WAXD frame, including exposure and readout of data, was 8.5 s.

WAXD images were processed with the software package FIT2D to obtain intensity versus scattering angle ($2\theta$) profiles. Crystallinity was calculated after deconvolution of the total intensity scattered by the crystalline ($A_{crystal}$) and amorphous ($A_{amorphous}$) domains:

$$X = \frac{A_{crystal}}{A_{crystal} + A_{amorphous}} \times 100\% \quad (2)$$

Flow-induced crystallization depends on the strength of the local flow field. In the slit geometry, the shear rate changes from a minimum in the center to a maximum at the wall, as shown in Figure 3, so shear-induced crystalline layers will form mostly next to the two walls. X-rays going through the whole sample thickness will scatter from the two shear layers, and therefore, values calculated in this way do not represent the real crystallinity in certain specific layer but rather an "apparent" crystallinity averaged over the optical path of the X-ray beam through whole sample.

## 3. RESULTS AND DISCUSSION

**3.1. Reference Experiment: No Pressure Quench after Flow.** The formation and development of flow-induced precursors are investigated with a shear pulse ($\dot{\gamma}_{wall} = 67$ $s^{-1}$, $t_{shear} = 0.8$ s) under 50 bar at 134 °C. First of all, the structural development during flow was examined through the rheological response of the polymer melt. Figure 4 shows the evolution of pressure difference during flow, which first increases rapidly, subsequently shows a small overshoot, and reaches a steady-state plateau. This behavior can be related to the usual nonlinear rheological response of the sheared molten polymer. Scelsi et al. reported a buildup of pressure difference (HDPE, 130 °C, $Wi$ for stretch is estimated around 60) during flow in a channel with a contraction in the middle section and associated

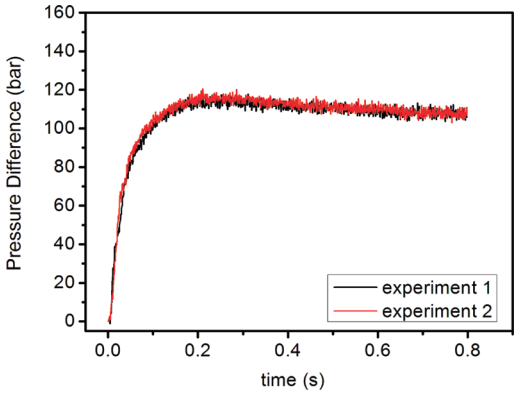


**Figure 4.** Pressure difference during flow. Two experiments are shown to demonstrate the reproducibility of the flow history.

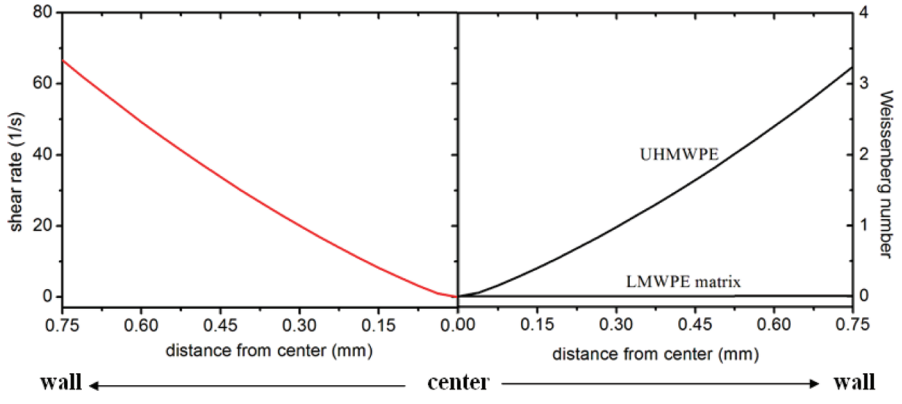


**Figure 3.** Distributions of shear rate and Weissenberg numbers for stretching HMW tail and LMW matrix over the slit thickness direction.


dx.doi.org/10.1021/ma2027325 | Macromolecules XXXX, XXX, XXX–XXX

it to continuous crystal formation concentrated in the region of slit exit.[40] Such a pressure difference buildup during flow was not observed in our experiments (134 °C, $Wi$ = 3.3). Therefore, our results imply that crystals do not form during flow or that the viscosity does not change even if precursors form (as discussed later).

Based on the nano- and mesoscale structures of crystalline planes and density differences, both SAXS and WAXD were employed to examine, at different length scales, structural aspects of flow-induced precursors. However, in-situ synchrotron SAXS and WAXD data acquired after flow did not show any observable signal, which confirms that no detectable crystallization takes place neither during flow nor within the next 20 min when the sample is kept isothermal (data not shown since no detectable signal was found). More in detail, despite the $Wi$ number for stretching, the HMW tail is larger than unity in the region close to the wall (see Figure 3); neither crystalline nor densely packed scatterers are observed. This can be a consequence of a low concentration of precursors, i.e., below the experimental detection limit. Therefore, crystallization has to be triggered to reflect the features of precursors. For PE, WAXD is sufficient to fulfill this purpose of characterizing crystallization features (i.e., orientation, crystallinity, twisted lamellae) which will be shown in the following results. Therefore, we use only WAXD[41] to track PE crystallization and show that a pressure quench is a suitable method to visualize precursors even at these very low concentrations.

**3.2. Pressure Quench after Flow.** In order to investigate the formation of flow-induced precursors, after the application of the same flow as in section 3.1, a pressure quench, with the pressure history shown in Figure 5, is performed. The pressure is raised linearly from the reference pressure of 50 to 300 bar without overshoot. The synchronous top and bottom pressures indicate that the pressure field is homogeneously distributed over the specimen and that there is no flow at the observation point (center of the slit). With pressure, undercooling is generated and immediately triggers crystallization, illustrated by the WAXD images in Figure 6.

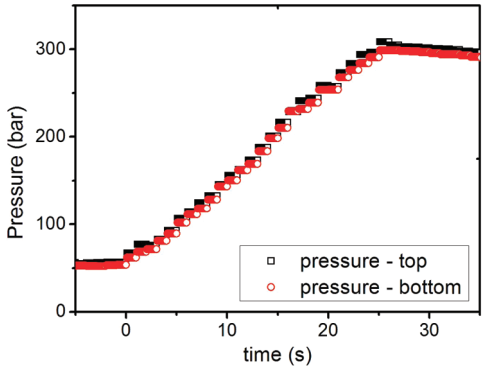


**Figure 5.** Pressure profile during a pressure quench.

As soon as the maximum pressure is approached, arched (110) and (200) reflections appear in the equator direction (Figure 6a), indicating the formation of the orthorhombic unit cell with $c$-axis aligned in the flow direction. According to Keller et al.,[6] the diffraction pattern of Figure 6a can be produced both by the extended chain crystals of shish and by the folded chain crystals of untwisted lamellae.

For the purpose of this paper, it is not essential to make such a distinction. The most important observation is the presence of highly oriented crystals. In fact, as the sample is pressurized in absence of flow, these oriented crystals originate from deformed molecules involved in precursors induced by flow.

As crystallization proceeds, the (110) reflection broadens in the azimuthal direction (Figure 6b) and, at $t_c$ = 17 s, splits into off-axis diffraction together with the clear appearance of off-axis (200) diffractions (Figure 6c). These off-axis (110) diffractions are the result of the lateral growth of twisted lamellae. During this process, the lamellar propagation direction holds perpendicular to the flow direction, but crystal units rotate along the $b$-axis.[6] Twisting leads to randomization in the orientation of $c$-axes. Keller et al.[6,42] proposed two extremes of lamellar orientation for flow-induced PE crystallization: "Keller/Machin I" and "Keller-Machin II". The former (KM-I) corresponds to the fully twisted lamellae producing off-axis (110) and meridional (200) diffractions. The latter refers to the flat, nontwisted lamellae (all $c$-axes parallel with flow direction) producing equatorial (110) and (200) diffractions. In the transition from one to another an "intermediate" state is observed showing the off-axis (110) and (200) patterns.[6,43] Therefore, the azimuthal features of the (200) diffraction reflect the lateral growth of lamellae.[6,9,43]

In a later stage, the diffraction of isotropic structures is also observed, e.g. isotropic (110), (200) diffractions at 102 s (see Figure 6d). These two crystallization processes, fast oriented crystallization and slow isotropic crystallization, characterized by different degrees of orientation and time scales can be rationalized by considering that the inhomogeneous flow field in the slit gives rise to inhomogeneous molecular stretch as shown by Figure 3. At the wall, where the stress reaches a maximum, molecules experience the largest stretch and many flow-induced precursors are generated. These are the domains

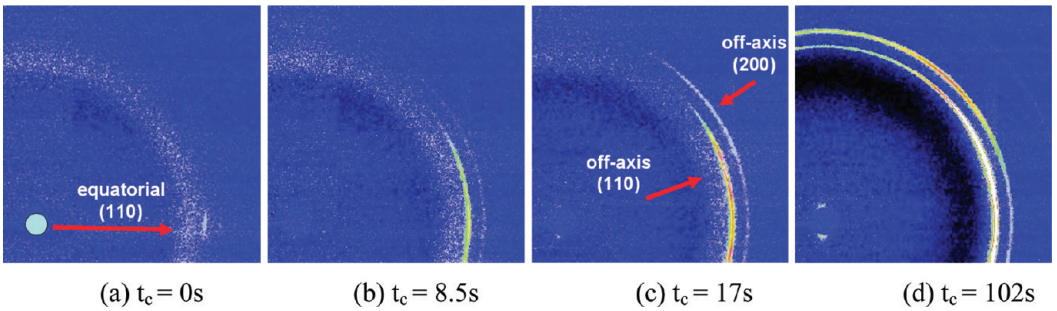


**Figure 6.** 2D WAXD patterns after a pressure quench after flow. $T$ = 134 °C; flow is in vertical direction. The reference time is the moment when 300 bar is reached.


dx.doi.org/10.1021/ma2027325 | Macromolecules XXXX, XXX, XXX–XXX

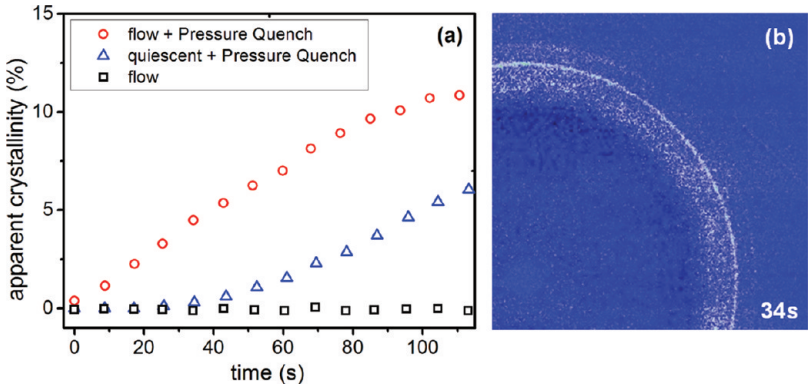


**Figure 7.** (a) Crystallinity evolution for shear-induced crystallization with pressure quench (○), quiescent crystallization with pressure quench (△), and shear-induced crystallization without pressure quench (□). (b) 2D WAXD pattern of quiescent crystallization under pressure quench at $t_c$ = 34 s and $T$ = 134 °C.

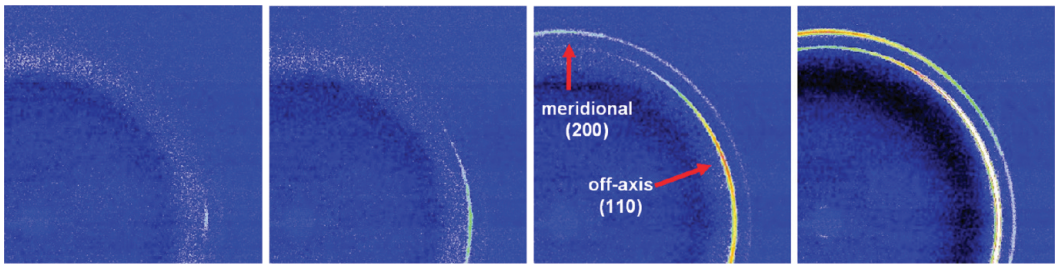


**Figure 8.** 2D WAXD patterns of structures after flow, 22 min annealing under 50 bar and a final pressure quench. Flow is along the vertical direction.

where highly oriented crystals are formed upon pressurization. Toward the centerline, molecules experience little or no stretch and the probability of forming oriented precursors vanishes. In this part of the sample, isotropic crystallization can be triggered purely by pressure. The WAXD images (Figure 6a–d) are indicative of structures averaged over the optical path of the X-ray beam (thickness of the samples), and therefore, they contain information on both these two processes.

Next, the effect of precursors on crystallization kinetics is illustrated in Figure 7a where the apparent crystallinity is plotted as a function of time for shear-induced crystallization under a pressure quench and two reference experiments (shear-induced crystallization without pressure quench and quiescent crystallization with pressure quench). It is evident that when shear is applied, crystallization starts as soon as the 300 bar pressure is reached. On the other hand, without shear, crystallization starts only after 25 s from reaching 300 bar. Eventually, without applying pressure, crystallization of the sheared polymer does not occur in the experimental time window of 20 min (see section 3.1 and Figure 7a). The results show that there is a remarkable interplay between flow and pressure on crystallization kinetics and morphology.

From the above results, we conclude that oriented precursors are generated by the flow, but prior to pressurization, they are invisible to X-rays (see section 3.1). It is clear that a pressure quench effectively provides the additional undercooling that triggers crystallization by raising the equilibrium melting temperature. The equilibrium melting temperature of PE at 1 bar is $T_m^0$ = 414.6 K.[44] Its increase with pressure, described by the Clausius–Clapeyron relation, can approximated by $T(p) = T_m^0 + (dT_m^p/dp)\Delta p$, where $dT_m^p/dp$ = 35.2 K/kbar.[44] In this way, the equilibrium melting temperatures corresponding to 50 and 300 bar are calculated as 416.4 and 425.2 K, respectively. With pressurization from 50 to 300 bar, the undercooling $\Delta T_{exp}^p = T_m^p - T_{exp}$ increases from $\Delta T_{134}^{50\ bar} \approx 9$ K to $\Delta T_{134}^{300\ bar} \approx 18$ K (experimental temperature 407.15 K). Thus, a pressure quench from 50 to 300 bar increases the undercooling by 9 K within 25 s. Such a pressure quench, around 22 K/min, is comparable to a temperature quench in small lab-scale device. On the other hand, it is much more efficient than lowering the temperature of such large metal device with a cooling medium, especially since the cooling rate decreases when approaching the target temperature, and thus it usually takes much longer time (minutes) to stabilize at the desired undercooling (see the Supporting Information).

The azimuthally homogeneous (110) diffraction in Figure 7b shows pressurizing does not cause flow at the observation point that could influence crystallization.

Concluding, oriented crystals (Figure 6) and faster kinetics (Figure 7a) show that precursors can form in a sheared melt, where only the HMW chain is stretched. This demonstrates that the HMW tail determine the formation precursors, consistent with the findings of Mykhaylyk et al.[15] A pressure quench triggers crystallization and effectively "lightens up" these flow-induced precursors which could not be detected otherwise for these conditions (134 °C, 50 bar).

**3.3. Pressure Quench after Annealing.** The effect of partial dissolution of flow-induced precursors can be semi-qualitatively estimated introducing an annealing step (during which pressure is kept at 50 bar) between the flow pulse and the pressure quench. During the annealing step, whose length is arbitrarily fixed at 22 min, no structural changes were observed by SAXS/WAXD (data not shown). Figure 8 shows the 2D WAXD patterns after applying a pressure quench to the sheared


dx.doi.org/10.1021/ma2027325 | Macromolecules XXXX, XXX, XXX–XXX

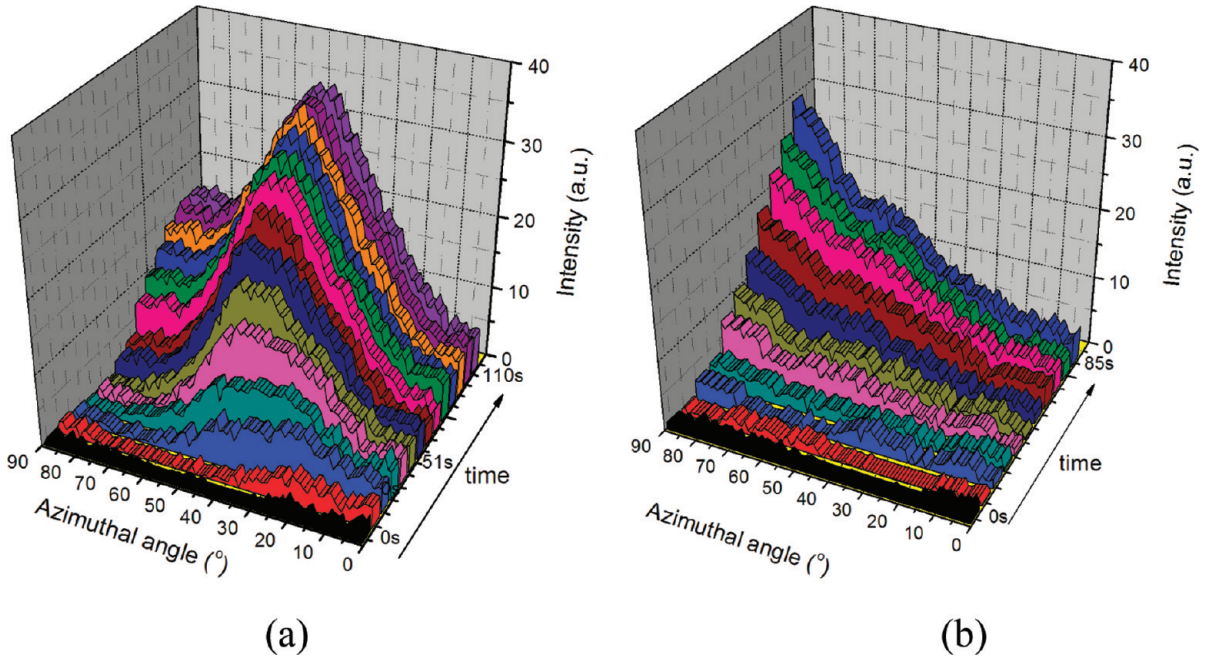


**Figure 9.** Change in the azimuthal distribution of (200) diffraction during pressure quench crystallizations for (a) unannealed and (b) an annealed sample.

and annealed specimen. The equatorial (110) diffraction in Figure 8a indicates the survival of orientation in the precursors with annealing.

The difference with crystallization without annealing (section 3.2) is the meridional (200) diffractions (Figure 8c) that arises from a higher degree of randomization in the *c*-axes of the unit cells.[6] This arises from the fact that, in the annealed sample, the lamellae can grow laterally over a longer distance; i.e., their nucleation points are further apart than in the nonannealed sample and also means that the annealed sample has a lower nucleation density.

This observation suggests that the lifetime of some of the flow-induced precursors is longer than 22 min (at 134 °C and 50 bar), whereas for others it is not.

The question is whether the long lifetime of precursor relates to the rheological time scales of the material. Considering the molecular weight between entanglements $M_e$ = 828 g/mol,[45] the numbers of entanglements per chain, $Z$, for HMW tail and LMW matrix are 1787 and 54, respectively. Because of the significant degree of overlap of long molecules and of the low Struglinski–Graessley number $Gr = Z_{HMW}/Z_{LMW}^3 = 0.01$, dynamic tube dilution can be neglected.[45] In other words, the relaxation time of HMW molecules is not reduced by the LMW matrix. According to the tube model, the Rouse time $\tau_{Rouse}$ and reptation time $\tau_D$, responsible for stretch and orientation relaxations, can be calculated from

$$\tau_{Rouse} = \tau_e Z^2 \tag{3}$$

$$\tau_D = 3\tau_e Z^3\left(1 - \frac{1.51}{\sqrt{Z}}\right)^2 \tag{4}$$

where $\tau_e$ is the entanglement equilibration time, around $7 \times 10^{-9}$ s for PE at 190 °C.[45] Without considering molecular weight distribution and the effect of 50 bar pressure, the estimated reptation times of the HMW tail and LMW matrix at 134 °C ($E_a$ = 21.8 kJ/mol) are 243 and 0.005 s, respectively, and the Rouse times are $4.9 \times 10^{-2}$ and $4.5 \times 10^{-5}$ s, respectively. The striking feature is that the longest relaxation time, $\tau_{D-HMW} \sim 4$ min (predicted with $M_w$), is much shorter than the annealing time, 22 min.

Concerning precursor relaxation, previous experimental studies[16,37,46] showed that the relaxation of the most unstable "shear-induced bundles", observable with SAXS, follows the reptation dynamics of the longest chains whereas stable precursors survive on time scales much longer than the rheological ones.

Systematical studies on "relaxing" shear-induced "nucleation precursors" that are invisible to SAXS were done by Alfonso and co-workers.[14] They found that, in iPP, at temperatures as high as 190 °C (above nominal melting temperature but not beyond equilibrium melting temperature), "nucleation precursors" can survive much longer than the longest rheological relaxation times, and that the characteristic survival time can be increased by a stronger or longer flow. The difference in relaxation times implies that other effects are determining the dissolution of precursors. This idea is supported by the different relaxation behaviors of the flow-induced helices in iPP as observed by Li et al.[46] They suggested that interactions between flow-induced helices of iPP dominate the dissolution rates and the helices with interactions relax slower than those without.

Considering the long lifetime of X-ray unobservable oriented precursors, in our results, it is reasonable to infer that interactions between PE chain segments (comparable to very local crystallization events) contribute to the long lifetime beyond the rheological times. According to the classical nucleation theory, a precursor below the critical size tends to relax; the interaction decreases the relaxation kinetics. Once the total interaction (contributed by the increased volume as well) is sufficient, the volume free energy overcomes the surface energy, and the precursors can develop to nuclei that are stable. Long-term stable precursors were also observed by Mykhaylyk et al.[15] for hydrogenated polybutadiene; the precursors survived


dx.doi.org/10.1021/ma2027325 | *Macromolecules* XXXX, XXX, XXX–XXX

within the experimental window which was as long as 10 h. Interestingly, in our experiments, when these segmental interactions are initiated during flow, they do not cooperate significantly to change the viscosity of the whole melt as observed from the pressure difference in the presence of precursors (see Figure 4).

The structures surviving the 22 min annealing step show some specific features that can be captured by looking at the (200) reflection. Figure 9a shows that the (200) diffraction of the unannealed sample occurs at low azimuthal angle and moves toward higher value with time. After about 51 s, the majority of the (200) diffractions tends to develop around the azimuthal angle of 50°, quite similar to the "intermediate" orientation mode. In contrast, for annealed samples, the (200) diffraction is found along the meridional direction (see Figure 9b), indicating a pronounced Keller/Machin I mode. The data of Figure 9 show that, during crystallization without annealing, a higher fraction of flat lamellae formed in comparison with the annealed sample.

The different morphology must be associated with nuclei density which is larger in the unannealed sample. This result is consistent with the finding of Keum et al.[9] that twisted lamellae are more prominent when the shish density is smaller due to lower shear strength (at the lower shear rate 20 $s^{-1}$ compared with 70 $s^{-1}$ for the same flow time). Thus, the lower nuclei density in the annealed sample indicates that some unstable shear-induced precursors relaxed during annealing. The specific diffraction pattern and crystallinity developments of the annealed and unannealed samples are compared in Figure 10 with quiescent crystallization as reference. The lower crystallinity in the annealed sample confirms the decrease in the total nuclei number, consistent with 2D patterns comparison between Figures 6 and 8.

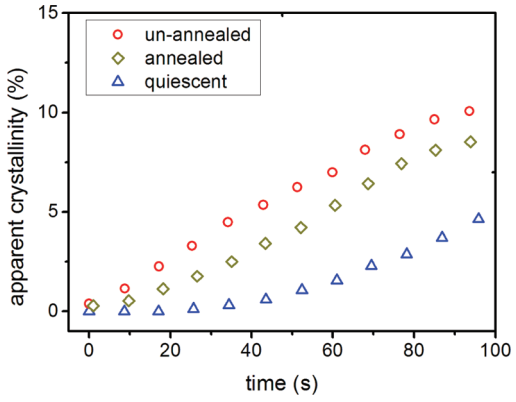


**Figure 10.** Crystallinity evolution for (○) unannealed, (◇) annealed, and (△) quiescent crystallization under pressure quench.

Concluding, both stable and unstable precursors are generated by the flow in a slit with varying flow strength over the thickness. The stable precursors orient and accelerate the following crystallization while unstable ones disappear during annealing leading to a larger space for overgrowth and higher fraction of twisted lamellae. These precursor evolutions, i.e., survival and relaxation, can be distinguished only by crystallization started with high enough undercooling, which, in this work, is obtained by a pressure quench.

**3.4. Inverse Quench by Depressurization.** Finally, we present the results for resetting the pressure from 300 bar back to 50 bar before reaching complete crystallization. Depressurization suddenly eliminates the increased undercooling (the experimental temperature is kept 134 °C). Figure 11a shows crystallinity evolutions after depressurization (prior to depressurization the annealed and unannealed sample have been crystallized for about 100 s). For both samples, crystallinity decreases but does not vanish completely. The residual crystallinity in unannealed sample is around 2%, 4 times larger than that of the annealed sample (final level around 0.5%). Crystallinity decrease after depressurization is ascribed to melting of the lamellae due to the reduced undercooling by depressurizing, which acts as "inverse quench".[47]

Cho et al.[48] suggested that PE lamellae may further thicken in an isothermal process. Thus, when the crystallization time is not long enough for all crystals to finish thickening, as in our work, the early formed crystals have thicker lamellae compared to those created in the late stages. The resulting lamellar distribution leads to variation in thermal stability. Thus, after depressurization the stable (thick) crystals can survive but unstable (thin) ones melt. As a result, the unannealed sample with more nuclei has more stable (thicker) crystals than the annealed sample. Figure 10 shows that oriented crystallization sets in before unoriented crystallization; therefore, oriented crystals experience longer isothermal thickening, and this makes them more likely survive in inverse quenching. This is confirmed by the results shown in Figure 11c.

## 4. CONCLUSIONS

The pressure quench is a relatively simple way to mimic a temperature quench. It has a number of advantages compared to thermal quenching (reverse cooling by depressurizing,

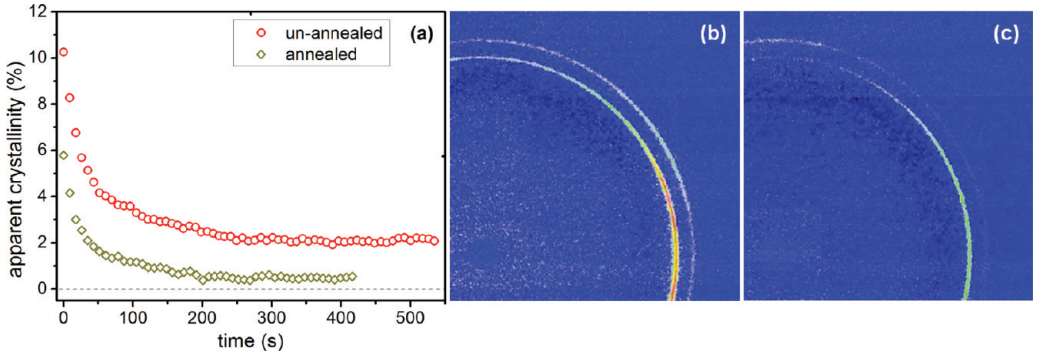


**Figure 11.** (a) Crystallinity evolution of (○) unannealed and (◇) annealed samples during melting. $t = 0$ when pressure reaches 50 bar. The last 2D WAXD images of (b) unannealed sample at 527 s and (c) annealed sample at 408 s during melting.


dx.doi.org/10.1021/ma2027325 | Macromolecules XXXX, XXX, XXX–XXX

avoiding temperature gradients, introducing complex thermal histories). It was applied for (a) crystallizations under quiescent condition and (b) flow and with and without subsequent annealing. For quiescent crystallization it is demonstrated that rising pressure to 300 bar is enough to trigger crystallization. Application on sheared samples shows that a pressure quench effectively visualizes the shear-induced precursors which are invisible to X-ray scattering. Crystallization kinetics is faster in this case, and oriented morphology is observed. The orientation in the outmost layer can survive annealing for 22 min, but the average nuclei density along the whole sample does relax. In addition, depressurization before crystallization leads to partially melting of the crystals which is explained by the variation in lamellar stability.

## ■ ASSOCIATED CONTENT

### Supporting Information

Experimental details. This material is available free of charge via the Internet at http://pubs.acs.org.

## ■ AUTHOR INFORMATION


### Corresponding Author

*Tel +31(0)402474840, e-mail g.w.m.peters@tue.nl.

### Present Address

[§]DSM Ahead, Urmonderbaan 22, Geleen 6167RD, The Netherlands.


### Notes

The authors declare no competing financial interest.

## ■ ACKNOWLEDGMENTS


We appreciate the helpful discussions with Prof. S. Rastogi (Eindhoven University of Technology) and Prof. G. C. Alfonso (University of Genova). We thank Dr. I. Vittorias (Basell Polyolefins, Germany) for providing the LMWPE matrix, Dr. MAG Jansen and C. Weijers (Department of Chemical Engineering, Eindhoven University of Technology) for the assistance with bimodal PE blending, and Dr. G. Portale (BM26, ESRF) for supporting the X-ray experiments.

NWO (Nederlandse Organisatie voor Wetenschappelijk Onderzoek) and ESRF are acknowledged for granting the beamtime.

This work is part of the Research programme of the Dutch Polymer Institute (DPI), P.O. Box 902, 5600 AX Eindhoven, The Netherlands, Project No. 714.


## ■ REFERENCES


(1) Meijer, H. E. H.; Govaert, L. E. *Prog. Polym. Sci.* **2005**, *30*, 915−938.

(2) Schrauwen, B. A. G.; Janssen, R. P. M; Govaert, L. E.; Meijer, H. E. H. *Macromolecules* **2004**, *37*, 6069−6078.

(3) Schrauwen, B. A. G.; van Breemen, L. C. A.; Spoelstra, A. B.; Govaert, L. E.; Peters, G. W. M.; Meijer, H. E. H. *Macromolecules* **2004**, *37*, 8618−8633.

(4) Kristiansen, M.; Werner, M.; Tervoort, T.; Smith, P.; Blomenhofer, M.; Schmidt, H. W. *Macromolecules* **2003**, *36*, 5150−5156.

(5) Eder, G.; Janeschitz-Kriegl, H. Structure development during processing: crystallization. In *Processing of Polymers*; Meijer, H., Ed.; Wiley-VCH: Weinheim, 1997; Vol. *18*, pp 269−342.

(6) Keller, A.; Kolnaar, H. W. H. Flow-induced orientation and structure formation. In *Processing of Polymers*; Meijer, H., Ed.; Wiley-VCH: Weinheim, 1997; Vol. *18*, pp 189−268.

(7) Kumaraswamy, G. *J. Macromol. Sci., Part C: Polym. Rev.* **2005**, *45*, 375−397.

(8) Somani, R. H.; Yang, L.; Zhu, L.; Hsiao, B. S. *Polymer* **2005**, *46*, 8587−8623.

(9) Keum, J. K.; Burger, C.; Zuo, F.; Hsiao, B. S. *Polymer* **2007**, *48*, 4511−4519.

(10) Fernandez-Ballester, L.; Gough, T.; Meneau, F.; Bras, W.; Ania, F.; Balta-Calleja, F. J.; Kornfield, J. A. *J. Synchrotron Radiat.* **2008**, *15*, 185−190.

(11) Alfonso, G. C.; Scardigli, P. *Macromol. Symp.* **1997**, *118*, 323−328.

(12) Azzurri, F.; Alfonso, G. C. *Macromolecules* **2005**, *38*, 1723−1728.

(13) Azzurri, F.; Alfonso, G. C. *Macromolecules* **2008**, *41*, 1377−1383.

(14) Cavallo, D.; Azzurri, F.; Balzano, L.; Funari, S. S.; Alfonso, G. C. *Macromolecules* **2010**, *43*, 9394−9400.

(15) Mykhaylyk, O. O.; Chambon, P.; Impradice, C.; Fairclough, J. P. A; Terrill, N. J.; Ryan, A. J. *Macromolecules* **2010**, *43*, 2389−2405.

(16) Balzano, L.; Kukalyekar, N.; Rastogi, S.; Peters, G. W. M.; Chadwick, J. C. *Phys. Rev. Lett.* **2008**, *100*, 048302.

(17) Housmans, J. W.; Balzano, L.; Santoro, D.; Peters, G. W. M.; Meijer, H. E. H. *Int. Polym, Proc.* **2009**, *24*, 185−197.

(18) Hammouda, B.; Balsara, N. P.; Lefebvre, A. A. *Macromolecules* **1997**, *30*, 5572−5574.

(19) Lefebvre, A. A.; Lee, J. H.; Jeon, H, S.; Balsara, N. P.; Hammouda, B. *J. Chem. Phys.* **1999**, *111*, 6082−6099.

(20) Van Meerveld, J.; Peters, G. W. M.; Hütter, M. *Rheol. Acta* **2004**, *44*, 119−134.

(21) Seki, M.; Thurman, D. W.; Oberhauser, J. P.; Kornfield, J. A. *Macromolecules* **2002**, *35*, 2583−2594.

(22) Heeley, E. L.; Fernyhough, C. M.; Graham, R. S.; Olmsted, P. D.; Inkson, N. J.; Embery, J.; Groves, D. J.; McLeish, T. C. B.; Morgovan, A. C.; Meneau, F.; Bras, W.; Ryan, A. J. *Macromolecules* **2006**, *39*, 5058−5071.

(23) Mykhaylyk, O. O.; Chambon, P.; Graham, R. S.; Fairclough, J. P. A; Olmsted, P. D.; Ryan, A. J. *Macromolecules* **2008**, *41*, 1901−1904.

(24) Vleeshouwers, S.; Meijer, H. E. H. *Rheol. Acta* **1996**, *35*, 391−399.

(25) Yang, L.; Somani, R. H.; Sics, I.; Hsiao, B. S.; Kolb, R.; Fruitwala, H.; Ong, C. *Macromolecules* **2004**, *37*, 4845−4859.

(26) Acierno, S.; Palomba, B.; Winter, H. H.; Grizzuti, N. *Rheol. Acta* **2003**, *42*, 243−250.

(27) Balzano, L.; Rastogi, S.; Peters, G. W. M. *Macromolecules* **2011**, *44*, 2926−2933.

(28) Rastogi, S.; Hikosaka, M.; Kawabata, H.; Keller, A. *Macromolecules* **1991**, *24*, 6384−6391.

(29) Hikosaka, M.; Tsukijlma, K.; Rastogi, S.; Keller, A. *Polymer* **1992**, *33*, 2502−2507.

(30) Roozemond, P. C.; Steenbakkers, R. J. A.; Peters, G. W. M. *Macromol. Theory Simul.* **2011**, *20*, 93−109.

(31) Janeschitz-Kriegl., H. *Colloid Polym. Sci.* **2003**, *281*, 1157−1171.

(32) Janeschitz-Kriegl, H.; Ratajski, E. *Polymer* **2005**, *46*, 3856−3870.

(33) Huang, R. PhD Thesis, Eindhoven University of Technology, The Netherlands, 2008.

(34) de Gennes, P. G. *Scaling Concepts in Polymer Physics*; Cornell University Press: Ithaca, NY, 1979.

(35) Takahashi, Y.; Isono, Y.; Noda, I.; Nagasawa, M. *Macromolecules* **1985**, *18*, 1002−1008.

(36) Schelten, J.; Ballard, D. G. H.; Wignall, G. D.; Longman, G.; Schmatz, W. *Polymer* **1976**, *17*, 751−757.

(37) Balzano, L.; Cavallo, D.; Van Erp, T. B.; Ma, Z.; Housmans, J. W.; Fernandez-Ballester, L.; Peters, G. W. M. *J. IOP Conf. Ser.: Mater. Sci. Eng.* **2010**, *14*, 012005/1−7.

(38) Mackley, M. R.; Marshall, R. T. J.; Smeulders, J. B. A. F. *J. Rheol.* **1995**, *39*, 1293−1309.

(39) Steenbakkers, R. J. A.; Peters, G. W. M. *J. Rheol.* **2011**, *55*, 401−433.

(40) Scelsi, L.; Mackley, M. R. *Rheol. Acta* **2008**, *47*, 895−908.

(41) Both SAXS and WAXD were used to examine if any X-ray observable precursors form during flow and develop within the

following isothermal period. But, only WAXD was further used to track the crystallizations started with pressure.
(42) Keller, A.; Machin, M. J. *J. Macromol. Sci. Phys., Part B: Phys.* **1967**, *1*, 41−91.
(43) Nagasawa, T.; Matsumura, T.; Hoshino, S. *Appl. Polym. Symp.* **1973**, *20*, 295−313.
(44) Wunderlich, B. *Macromolecular Physics*; Academic Press: New York, 1980; Vol. 3.
(45) Dealy, J. M.; Larson, R. G. *Structure and Rheology of Molten Polymers*; Hanser Gardner Pubs: Cincinnati, 2006.
(46) Phillips, A. W.; Bhatia, A.; Zhu, P.; Edward, G. *Macromolecules* **2011**, *44*, 3517−3528.
(47) An, H.; Li, X.; Geng, Y.; Wang, Y.; Wang, X.; Li, L.; Li, Z.; Yang, C. *J. Phys. Chem. B* **2008**, *112*, 12256−12262.
(48) Acierno, S.; Grizzuti, N. *J. Rheol.* **2003**, *47*, 563−576.
(49) Cho, T.; Heck, B.; Strobl, G. *Colloid Polym. Sci.* **2004**, *282*, 825−832.